TBC1D5 controls the GTPase cycle of Rab7b

Distefano, M.B.; Haugen, L.H.; Wang, Y.; Perdreau-Dahl, H.; Kjos, I.; Jia, D.; ... ; Progida, C.

RESEARCH ARTICLE

TBC1D5 controls the GTPase cycle of Rab7b

Marita Borg Distefano[1], Linda Hofstad Haugen[1], Yan Wang[2,*], Harmonie Perdreau-Dahl[3,*], Ingrid Kjos[1], Da Jia[2], Jens Preben Morth[3,4], Jacques Neefjes[5], Oddmund Bakke[1,‡] and Cinzia Progida[1,‡]

ABSTRACT

Rab GTPases are key regulators of intracellular trafficking, and cycle between a GTP-bound active state and a GDP-bound inactive state. This cycle is regulated by guanine-nucleotide exchange factors (GEFs) and GTPase-activating proteins (GAPs). Several efforts have been made in connecting the correct GEFs and GAPs to their specific Rab. Here, we aimed to identify GAPs for Rab7b, the small GTPase involved in transport from late endosomes to the trans-Golgi. An siRNA screen targeting proteins containing TBC domains critical for Rab GAPs was performed and coupled to a phenotypic read-out that visualized the distribution of Rab7b. Silencing of TBC1D5 provided the strongest phenotype and this protein was subsequently validated in various *in vitro* and cell-based assays. TBC1D5 localizes to Rab7b-positive vesicles, interacts with Rab7b and has GAP activity towards Rab7b *in vitro*, which is further increased by retromer proteins. Similarly to the constitutively active mutant of Rab7b, inactivation of TBC1D5 also reduces the number of CI-MPR- and sortilin-positive vesicles. Together, the results show that TBC1D5 is a GAP for Rab7b in the control of endosomal transport to the trans-Golgi.

This article has an associated First Person interview with the first author of the paper.

KEY WORDS: Rab7b, Rab proteins, GAP, GTPase, TBC domains, Endosomes, Trans-Golgi

INTRODUCTION

Rab proteins are the master regulators of intracellular trafficking; they coordinate vesicle transport in the cell and ensure that specific cargoes are delivered to their correct destinations (Pylypenko et al., 2017). Rab proteins are small GTPases that cycle between two conformational states: an inactive GDP-bound state and an active GTP-bound state. The conversion from an inactive to active state is promoted by a guanine nucleotide exchange factor (GEF), which catalyses the exchange of GDP for GTP. This switch is coupled to membrane insertion, and normally, when Rabs are recruited to membranes, they can interact with effector proteins (Stenmark, 2009).

[1]Department of Biosciences, Centre for Immune Regulation, University of Oslo, 0316 Oslo, Norway. [2]Key Laboratory of Birth Defects and Related Diseases of Women and Children, Department of Paediatrics, West China Second University Hospital, State Key Laboratory of Biotherapy, Sichuan University, Chengdu 610041, China. [3]Norwegian Center of Molecular Medicine, Nordic EMBL Partnership, University of Oslo, 0318 Oslo, Norway. [4]Institute for Experimental Medical Research, Oslo University Hospital, 0424 Oslo, Norway. [5]Department of Cell and Chemical Biology, Leiden University Medical Center LUMC, 2300 RC Leiden, The Netherlands.
*These authors contributed equally to this work

‡Authors for correspondence (c.a.m.progida@ibv.uio.no; oddmund.bakke@ibv.uio.no)

Y.W., 0000-0003-2343-8366; D.J., 0000-0002-2205-1998; J.P., 0000-0003-4077-0192; J.N., 0000-0001-6763-2211; O.B., 0000-0003-4843-7626; C.P., 0000-0002-9254-0690

GTPase-activating proteins (GAPs) promote the intrinsic GTPase activity of Rab proteins, and thus the inactive Rab is released into the cytosol. Cycling between GTP-bound and GDP-bound forms is crucial for the role of Rab proteins in regulating vesicular trafficking and most of them preferentially interact with effector molecules when they are in the GTP- and thus membrane-bound form (Grosshans et al., 2006; Muller and Goody, 2017; Stenmark, 2009).

The small GTPase Rab7b localizes to late endosomes/lysosomes, and to the Golgi and *trans*-Golgi network (TGN), and regulates intracellular traffic from late endosomes towards the Golgi (Progida et al., 2010). Indeed, Rab7b controls the retrograde transport of different sorting receptors such as the cation-independent mannose-6-phosphate receptor (CI-MPR) and sortilin (Progida et al., 2012). Rab7b was recently found to have additional roles in the cell, as it is involved in both autophagy (Kjos et al., 2017) and in modulating actomyosin-dependent processes such as cell migration by interacting directly with myosin II (Borg et al., 2014).

Previous results showed that the constitutively active mutant of Rab7b, Rab7b-Q67L, which is defective in GTP hydrolysis, impairs the formation of carriers containing sorting receptors from the TGN, indicating that the ability of Rab7b to hydrolyse GTP is important for the correct carrier formation at the TGN (Progida et al., 2012). To further elucidate the mechanisms used by Rab7b to regulate this process, we aimed to identify specific GAPs for this small GTPase. Proteins containing a Tre2, Bub2, Cdc16 (TBC) domain are broadly conserved in eukaryotes and function as GAPs for Rab GTPases (Pan et al., 2006). Therefore, we performed an siRNA screen targeting 36 different proteins containing a TBC domain expressed in MelJuSo cells, and selected seven proteins that altered the intracellular distribution of Rab7b when depleted.

We further characterized two of these TBC proteins, namely TBC1D5 and TBC1D10A, and found that TBC1D5, but not TBC1D10A, localizes to Rab7b-positive vesicles. TBC1D5 interacts with Rab7b and controls the GTPase cycle of Rab7b *in vitro*. In addition, we demonstrated by fluorescence recovery after photobleaching (FRAP) analysis that overexpression of TBC1D5, but not TBC1D10A, attenuated the Rab7b cycle at the Golgi and late endosomes, whereas depletion of TBC1D5 stabilized membrane-bound Rab7b. Finally, we also found that depletion of TBC1D5, similarly to the constitutively active mutant of Rab7b (Progida et al., 2012), significantly reduces the number of vesicles positive for CI-MPR and sortilin. In sum, TBC1D5 controls the Rab7b cycle and this is important for the regulation of the transport between endosomes and the Golgi.

RESULTS

An siRNA screen of putative GAPs for Rab7b

In order to identify a specific GAP for Rab7b, we performed an siRNA screen using an siRNA library targeting proteins containing a TBC domain. As Rab7b is highly expressed in immune cells (Yang et al., 2004), we chose siRNAs targeting 36 different TBC domain proteins highly expressed in monocyte-derived dendritic

cells and in the human melanoma cell line MelJuso (Table S1), which is often used as a model cell line for antigen-presenting cells (APCs) (Paul and Neefjes, 2013; Wubbolts et al., 1996). MelJuso cells stably expressing GFP-Rab7b were first transfected with pools of four different siRNAs per target gene. At 3 days post-transfection, the cells were fixed and immunostained for the late endosomal marker CD63 and the Golgi marker Giantin, and imaged by confocal microscopy to identify the siRNAs that altered the Rab7b phenotype in comparison to the cells treated with a non-targeting control siRNA (Fig. 1A). From the 36 siRNA pools, 18 siRNAs did not affect Rab7b distribution or localization, whereas four siRNAs gave inconsistent effects between experiments and seven siRNAs reduced cell viability. Ultimately, seven targets clearly affected Rab7b localization (Table S1). In comparison to the control, where Rab7b was localized to late endosomes and Golgi, the phenotypic differences for Rab7b were grouped in three different categories; (1) peripheral, (2) cytosolic and Golgi, or (3) clustered and enlarged distribution (Fig. 1B). The depletion of USP6, TBC1D2B, TBC1D22A or TBC1D25 resulted in a more peripheral distribution of Rab7b-positive vesicles (Fig. 1C). Depletion of TBC1D10A caused Rab7b to localize mainly in the perinuclear/Golgi region and at the same time to become more cytosolic, while depletion of TBC1D5 or TBC1D14 resulted in clustered and enlarged Rab7b-positive vesicles (Fig. 1C).

To validate the individual siRNAs and exclude off-target effects, we next tested each of the four oligos present in the pools of siRNAs that gave the strongest effects on Rab7b localization (Fig. 2A). From the deconvolution screen, we excluded 3 of the 7 targets (namely TBC1D2B, TBC1D22A and USP6), because of off-target effects and non-consistent results (Fig. S1, Table S2). Depletion of the remaining four candidates gave consistent results: similarly to the original siRNA screen, deconvolution of TBC1D14 and TBC1D25 caused enlargement and dispersion of Rab7b-positive vesicles, respectively (Fig. S1, Table S2). However, the knockdown of a specific GAP for Rab7b should cause a phenotype similar to that of the Rab7b constitutively active mutant, since both the active mutant and the depletion of a specific GAP causes an overall reduced GTPase activity of the Rab protein. As the constitutively active mutant of Rab7b localizes mainly to the Golgi (Progida et al., 2010, 2012), we searched for genes whose silencing resulted in a redistribution of Rab7b towards a more perinuclear localization. Silencing of TBC1D5 or TBC1D10A provided such a phenotype (Fig. 2B, Table S2). Moreover, three out of four siRNAs tested for each of the two TBC proteins gave comparable results. Also, in the case of TBC1D5, expression of mCherry-TBC1D5 in TBC1D5-depleted cells significantly rescued the effect of the silencing, thereby validating the specificity of the TBC1D5 silencing (Fig. S2A). For these two selected TBC proteins, we quantified the silencing efficiency of the two siRNAs with the most consistent effects on Rab7b distribution. As shown in Fig. 2C,D, the selected siRNAs resulted in an efficient silencing of their respective targets, with a ∼60% decrease in levels of TBC1D10A, and a ∼70% decrease in levels of TBC1D5, compared with levels in control cells.

In sum, using a targeted phenotypic siRNA screen, we identified two TBC domain-containing proteins affecting the intracellular distribution of Rab7b similarly to its constitutive active mutant and that therefore could be potential GAPs for Rab7b.

TBC1D5, but not TBC1D10A, localizes to Rab7b-positive vesicles

Since TBC1D5 and TBC1D10A depletion affects Rab7b intracellular localization in a similar way to the Rab7b

constitutively active mutant, we next investigated whether these GAPs colocalized with Rab7b. MelJuso cells were transiently transfected with mCherry-Rab7b together with either GFP-TBC1D10A or GFP-TBC1D5, and imaged with a spinning disk confocal microscope. In MelJuso cells, GFP-TBC1D10A was mostly cytosolic and on the plasma membrane, with no clear colocalization with Rab7b (Fig. S3A). Interestingly, TBC1D10A has been reported to induce accumulation of actin-coated vacuoles when overexpressed in HeLa cells (Hanono et al., 2006). Therefore, we transfected HeLa cells with mCherry-Rab7b and GFP-TBC1D10A and investigated whether the two proteins colocalize on these compartments. However, the actin-coated vesicles induced by TBC1D10A overexpression were not positive for Rab7b (Fig. S3B).

Next, we investigated the localization of mCherry-Rab7b and GFP-TBC1D5 in MelJuso cells. As shown in Fig. 3A, GFP-TBC1D5 is mostly cytosolic, but was occasionally present on domains of enlarged vesicles positive for Rab7b (Fig. 3A, Movie 1). We observed the same in HeLa cells co-transfected with GFP-TBC1D5 and mCherry-Rab7b, with both proteins present on the same endosomal vesicles in live cells (Fig. 3B, Movie 2). A similar co-localization was observed in fixed HeLa cells co-transfected with GFP-TBC1D5 and HA-Rab7b (Fig. S2B). Since a GAP needs to interact with its target Rab GTPase in order to inactivate it, TBC1D5 was the most plausible candidate as a Rab7b GAP. To test this, we subsequently validated the interaction between TBC1D5 and Rab7b by co-immunoprecipitation (Co-IP) with GFP-Trap magnetic beads. MelJuso cells were transiently transfected with GFP-TBC1D5 and HA-Rab7b-WT, the constitutively active mutant HA-Rab7b-Q67L or the dominant negative mutant HA-Rab7b-T22N. The latter was included to investigate if a potential interaction was dependent on the activation state of Rab7b. TBC1D5 co-immunoprecipitated only Rab7b-WT, but not its mutants (Fig. 3C). Thus, Rab7b and TBC1D5 are present on the same vesicles, and can interact, further supporting the hypothesis that TBC1D5 is a Rab7b GAP.

In vitro GAP activity of TBC1D5 and TBC1D10A towards Rab7b

One way to determine if TBC1D10A and TBC1D5 are specific GAPs for Rab7b is to measure the *in vitro* intrinsic GTPase activity of Rab7b and compare it with the GAP-stimulated GTPase-activity via a phosphate release bismuth activity assay (Mishra and Lambright, 2015). Therefore, we bacterially expressed and purified full-length Rab7b-WT, in addition to the constitutively active (Rab7b-Q67L) and dominant negative (Rab7b-T22N) mutants as controls (Fig. S3C). We loaded these constructs with GTP and determined the intrinsic GTPase activity of Rab7b and its mutants by measuring the amount of free phosphate released after 60 min, which is directly proportional to the activity of the GTPase (Cariani et al., 2004). The negative control (without Rab7b) showed no specific GTPase activity, while both Rab7b-WT and Rab7b-Q67L exerted significant GTPase activity, to a similar degree (6.5 and 6.75 nmol free Pi min^{-1} mg^{-1}, respectively). This is in line with previous results showing that some Rab proteins with Q-to-L mutations can retain the ability to hydrolyse GTP by basal hydrolysis reactions *in vitro*, while their GAP-stimulated hydrolysis is decreased (Gavriljuk et al., 2012; Langemeyer et al., 2014). As expected, the dominant negative mutant Rab7b-T22N had a significantly lower hydrolysis rate of GTP compared with that of Rab7b-WT, with only 3.67 nmol free Pi min^{-1} mg^{-1} (Fig. S3D). Altogether, this shows that Rab7b indeed has an intrinsic ability to hydrolyse GTP.
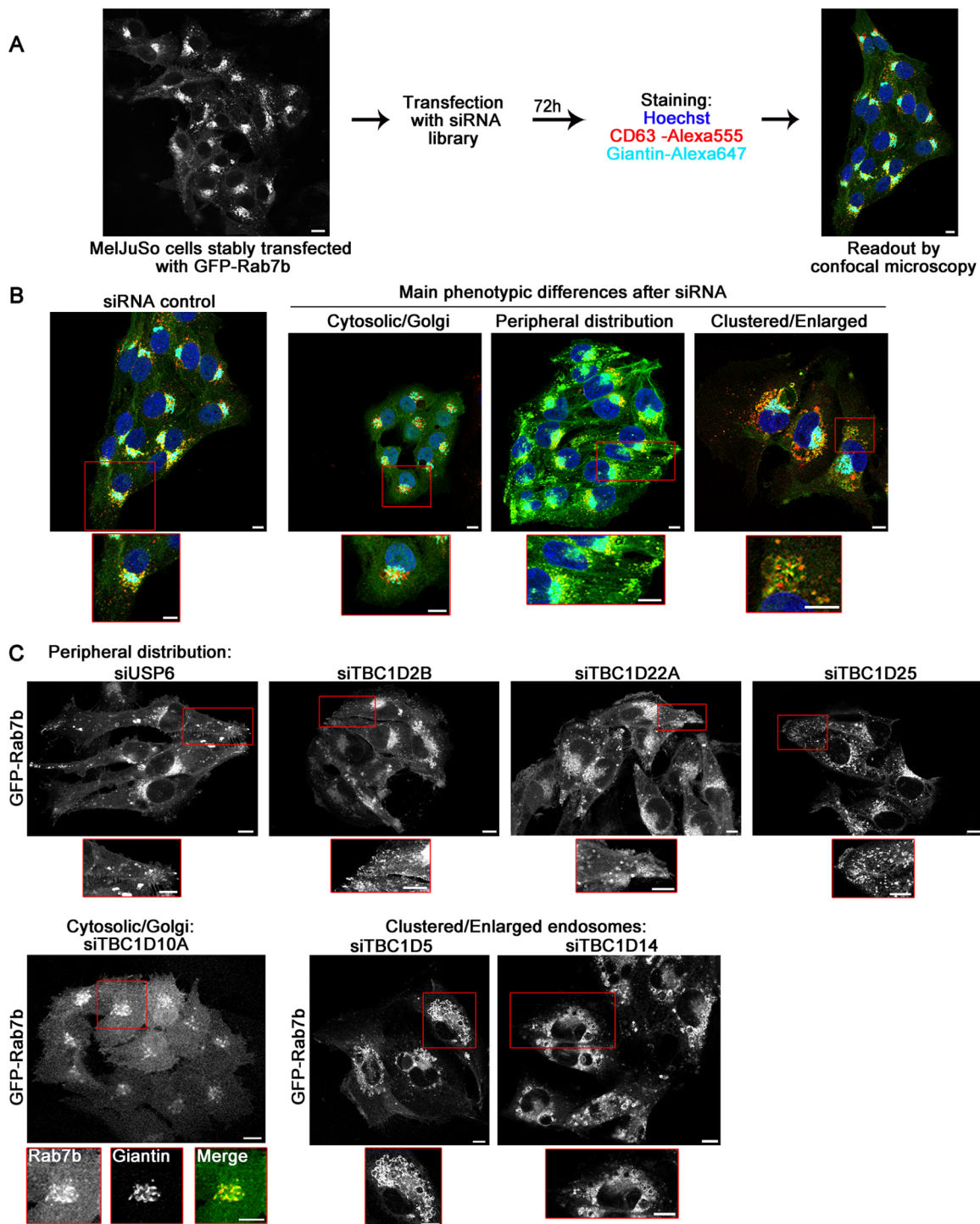
Fig. 1. siRNA screen to identify GAP proteins that affect Rab7b localization. (A) MelJuso cells stably expressing GFP-Rab7b were transfected with siRNA oligos targeting 36 different TBC domain-containing proteins, and stained for late endosomes (CD63-Alexa555, red), Golgi (Giantin-Alexa647, cyan) and nucleus (Hoechst 33258, blue), before readout by confocal microscopy. (B) Representative confocal images from the siRNA screen of the three main Rab7b phenotypes, in comparison to the control. (C) Representative confocal images of MelJuso cells stably expressing GFP-Rab7b silenced with the selected seven siRNA oligos from the siRNA screen. The results are divided into three groups according to the different Rab7b phenotypes: siRNAs resulting in a more peripheral distribution of Rab7b-positive vesicles (top), siRNAs causing a more cytosolic and Golgi distribution of Rab7b (bottom left) or siRNAs inducing clustering and enlargement of Rab7b-positive endosomes (bottom right). Scale bars: 10 μm.

A GAP specific for Rab7b is expected to accelerate the Rab7b intrinsic rate of GTP hydrolysis, and thus more free phosphate should be released (Barr and Lambright, 2010). In order to test whether TBC1D10A exerted GAP activity on Rab7b, we expressed TBC1D10A in *E. coli*. The purified protein was more than 90% pure (Fig. S3E). When we measured the *in vitro* GTPase activity, GTP by itself or TBC1D10A alone did not exert any significant GTP hydrolysis compared with Rab7b-WT (Fig. S3F).
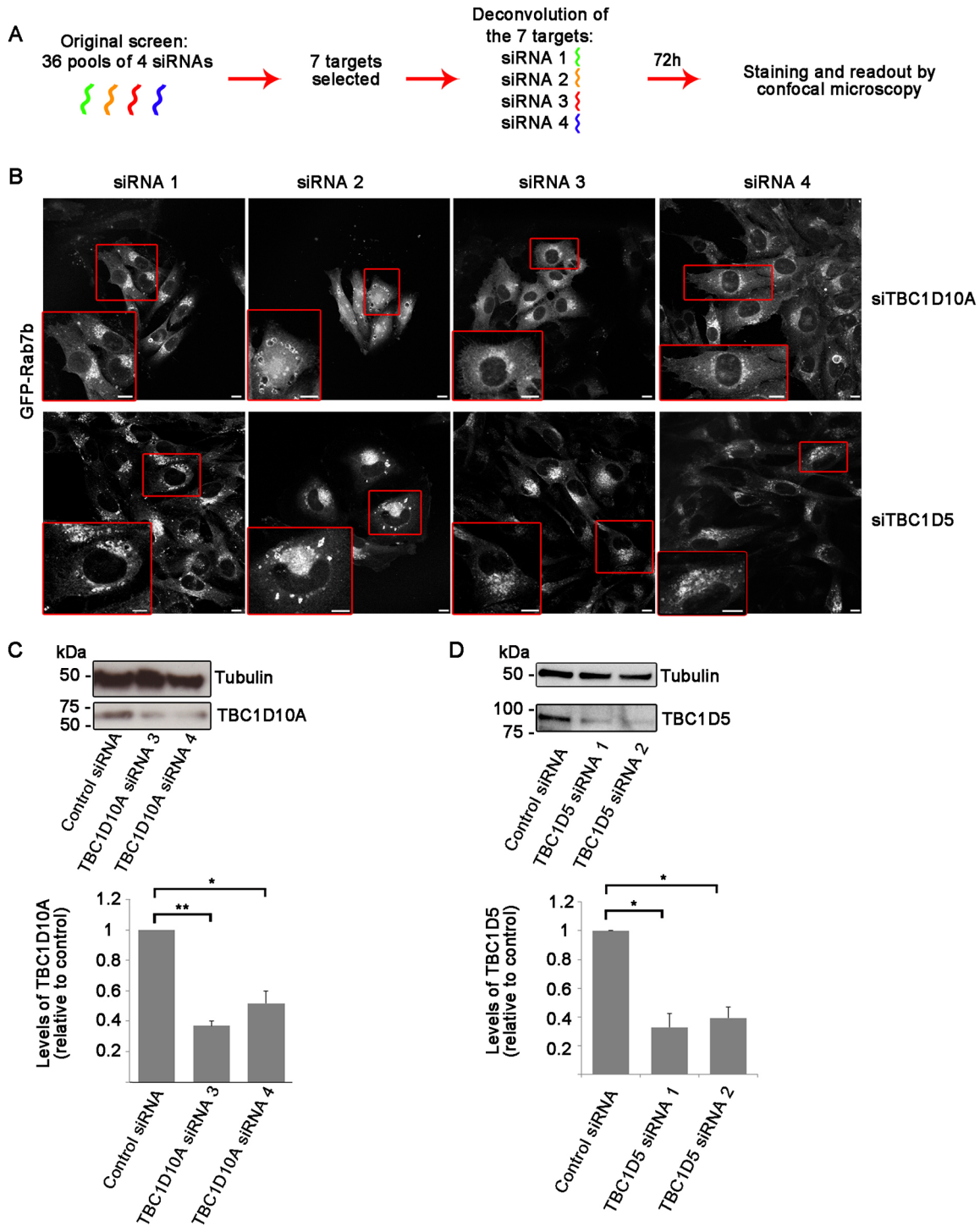
Fig. 2. Deconvolution of the hits from the siRNA primary screen. (A) A deconvolution screen was performed for selected hits similarly to the original siRNA screen, testing each of the four siRNAs individually instead of in pools. (B) Representative confocal images of MelJuso cells stably expressing GFP-Rab7b and silenced individually with each of the four siRNAs present in the pools targeting TBC1D10A (top) or TBC1D5 (bottom). The boxed areas are enlarged in insets. Scale bars: 10 μm. (C,D) Lysates from MelJuso cells transfected with control siRNA and siRNAs targeting different regions of TBC1D10A (C) or TBC1D5 (D) analyzed by western blotting with tubulin as a loading control (top). The intensities of the bands were quantified by densitometry, normalized to the amount of tubulin and plotted relative to the amount of TBC1D10A (C) or TBC1D5 (D) in the cells treated with control siRNA (bottom). Values are mean±s.e.m. of three independent experiments. Paired two-tailed Student's t-test, *$P<0.05$, **$P<0.01$.

Similarly, the addition of TBC1D10A to Rab7b-WT did not increase its intrinsic GTPase activity (Fig. S3F). This indicates that TBC1D10A is not a GAP for Rab7b.

To investigate whether TBC1D5 has GAP activity towards Rab7b, we took advantage of an existing system that has been

successfully used to identify TBC1D5 as a GAP for Rab7a (Jia et al., 2016; Mukhopadhyay et al., 2007). TBC1D5 was purified both alone and in complex with retromer subunits VPS35 and VPS29 (Fig. 4A). The purified proteins did not exert any GTP hydrolysis over time (Fig. 4B). In line with previously published
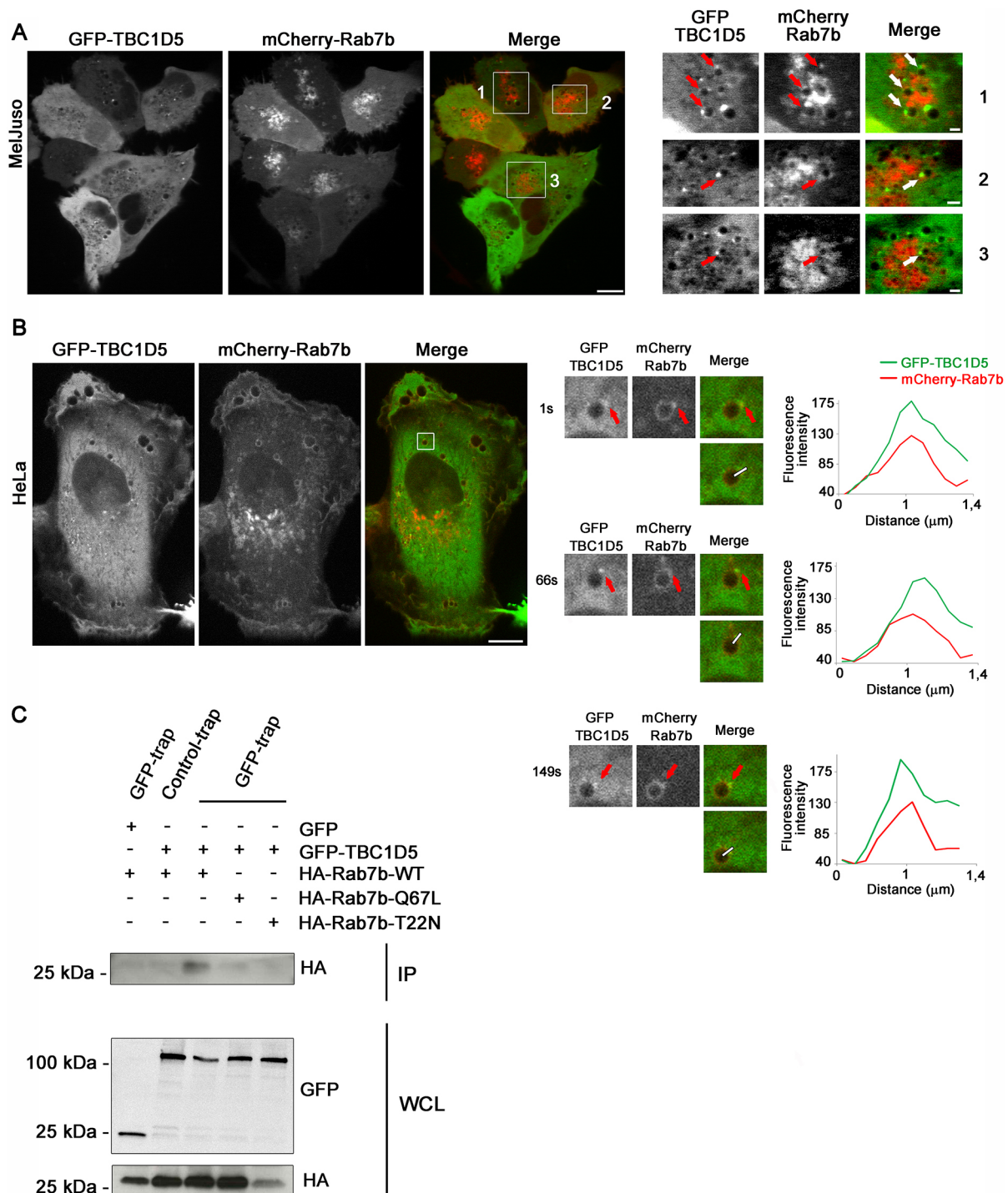
Fig. 3. TBC1D5 localizes to Rab7b-positive vesicles. (A) MelJuso cells transiently transfected with GFP-TBC1D5 (green) and mCherry-Rab7b (red) were imaged using a spinning disk microscope at 37°C and 5% CO_2. Scale bar: 10 µm. Boxed areas are enlarged on the right and arrows indicate vesicles positive for both GFP-TBC1D5 and mCherry-Rab7b. Scale bars: 2 µm. (B) HeLa cells transiently transfected with GFP-TBC1D5 (green) and mCherry-Rab7b (red) were imaged using a spinning disk microscope. Scale bar: 10 µm. The boxed area is enlarged and shows a vesicle positive for both TBC1D5 and Rab7b (red arrows) at 1 s, 66 s and 149 s time points (middle). Fluorescence intensity profiles along the white line for each channel are shown for each time point (right). (C) MelJuso cells were transiently co-transfected with HA-Rab7b-WT and GFP or with GFP-TBC1D5 and either HA-Rab7b-WT, HA-Rab7b-Q67L or HA-Rab7b-T22N, before lysis and immunoprecipitation with magnetic agarose GFP-TRAP beads. Whole cell lysates (WCL) and immunoprecipitates (IP) were subjected to western blot analysis with the indicated antibodies.

data, TBC1D5 promoted Rab7a GTP hydrolysis, and the addition of retromer to the reaction further augmented the GTPase activity of Rab7a (Fig. 4C), (Jia et al., 2016). Importantly, when we performed the *in vitro* GTPase activity assay for Rab7b, we observed that

TBC1D5 also promoted Rab7b GTP hydrolysis, and that Rab7b GTPase activity is higher in the presence of the retromer (Fig. 4D). Taken together, these data suggests that TBC1D5, but not TBC1D10A, is the actual GAP for Rab7b.
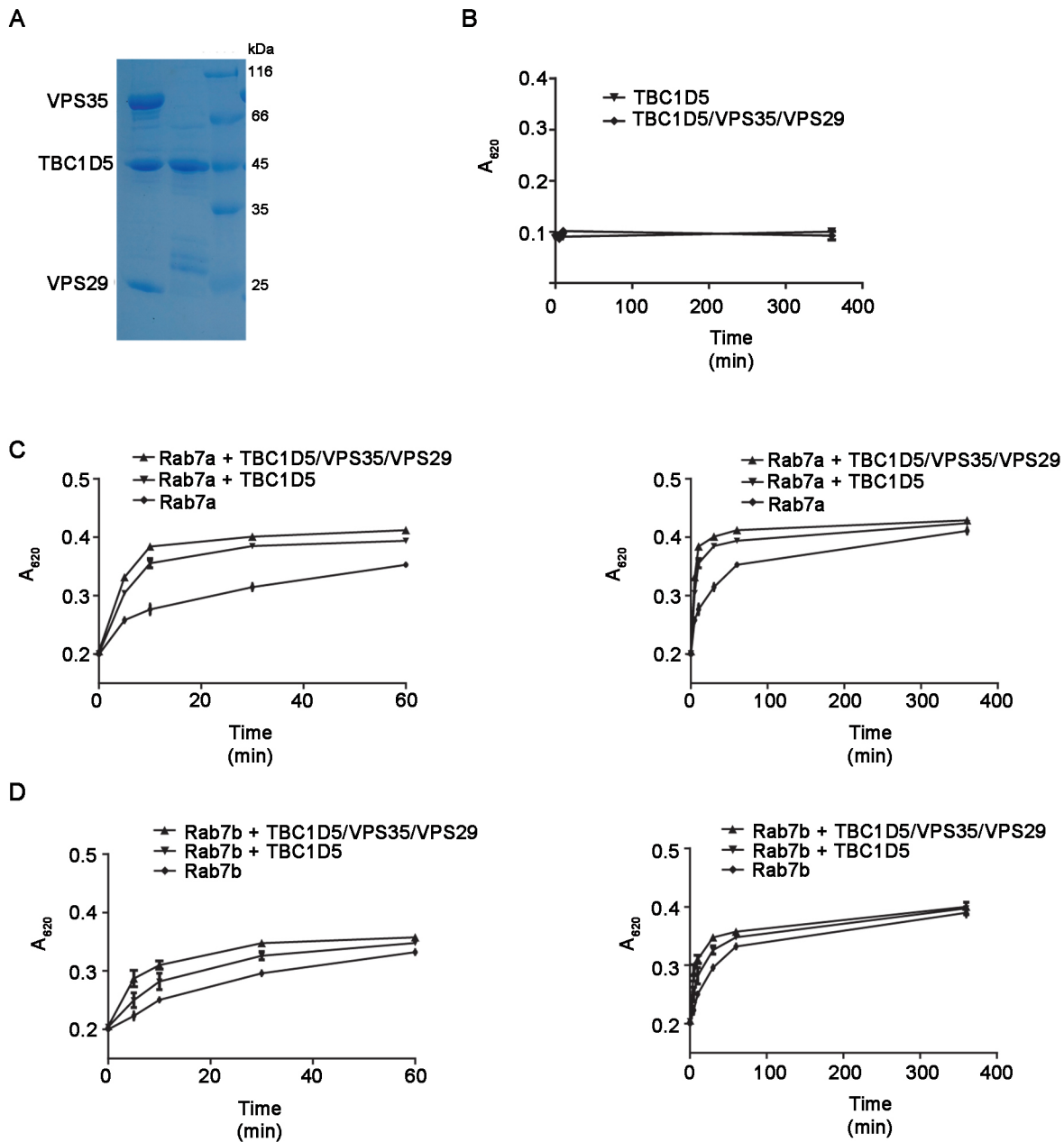
Fig. 4. TBC1D5 and the retromer promote GTP hydrolysis by Rab7b. (A) A Coomassie Blue-stained gel of purified TBC1D5 (amino acids 1-419) and the TBC1D5-VPS35-VPS29 complex. (B-D) Kinetics of GTP hydrolysis by TBC1D5 or TBC1D5-VPS35-VPS29 (B) and kinetics of GTP hydrolysis by Rab7a (C) or Rab7b (D) in the absence and presence of TBC1D5 or TBC1D5-VPS35-VPS29. The absorbance at 620 nm reports the amount of a conjugate of the GTP hydrolysis product, Pi. All values are presented as mean±s.e.m., derived from two independent experiments.

TBC1D5 delays the recovery of GFP-Rab7b at the Golgi and late endosomes, and influences membrane association of Rab7b

To further investigate if the binding kinetics of Rab7b to membranes was affected by the presence of TBC1D5, we used FRAP. Active Rab7b is recruited to late endosomes where it regulates the transport towards the TGN and Golgi (Progida et al., 2010), where Rab7b should be inactivated by its specific GAP. Therefore, if TBC1D5 is a GAP for Rab7b, it should influence Rab7b kinetics at the Golgi. To examine this, HeLa cells were transfected with either mCherry-Rab7b alone, or together with GFP-TBC1D5 or GFP-TBC1D10A (as a negative control). We performed FRAP on live cells by bleaching the entire pool of

GFP-Rab7b present in the Golgi, and monitoring the $t_{1/2}$ recovery of Rab7b with or without the putative GAPs (Fig. 5A). The FRAP analysis showed that Rab7b alone had a $t_{1/2}$ recovery of 19.01 ±0.57 s, while Rab7b together with TBC1D10A had a $t_{1/2}$ recovery of 26.25±0.87 s, indicating that overexpression of TBC1D10A did not affect Rab7b kinetics (Fig. 5B,C). Intriguingly, when Rab7b was co-expressed with TBC1D5, the $t_{1/2}$ recovery significantly slowed down to 162.90±4.99 s (Fig. 5B,C). Notably, the slower recovery of Rab7b at the Golgi in the presence of TBC1D5 suggests that Rab7b membrane-to-cytosol cycling is dependent on TBC1D5. This further supports the conclusion that TBC1D5, but not TBC1D10A, functions as a regulator of Rab7b GTPase activity.
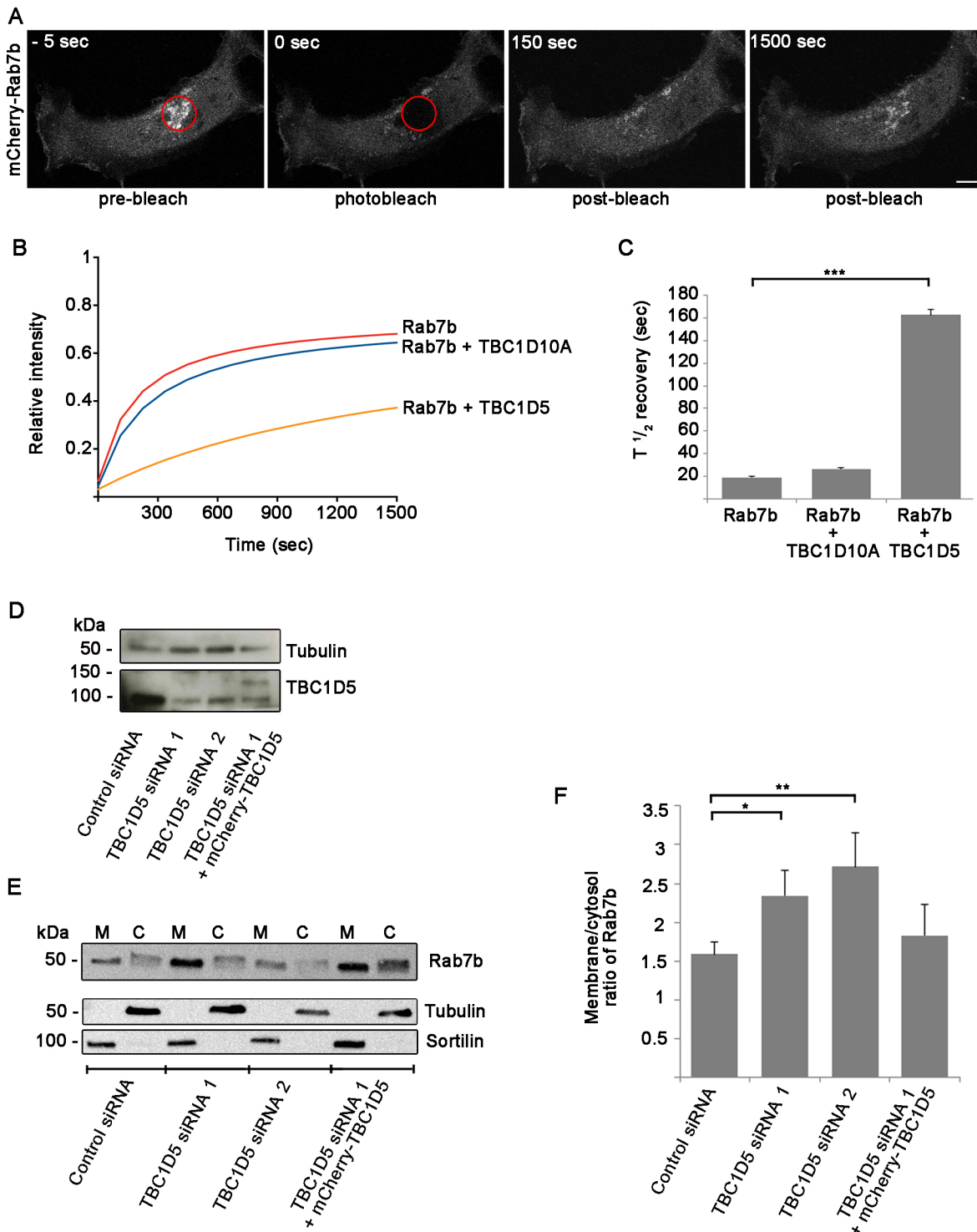
Fig. 5. Rab7b membrane kinetics is dependent on TBC1D5. (A) HeLa cells transfected with mCherry-Rab7b imaged before (pre-bleach), during and after photobleaching the Golgi region (outlined in red). Scale bar: 10 µm. (B) Total linear fitted recovery curves for mCherry-Rab7b from 15 independent experiments for each condition. Curves show the recovery in the ROI over time of Rab7b in control cells (red), Rab7b in cells transfected with TBC1D10A (blue) and Rab7b in cell transfected with TBC1D5 (yellow). For clarity, error bars are not shown. (C) Histogram of the $t_{1/2}$ recovery from FRAP analysis. Values are mean±s.e.m. of 15 independent experiments for each condition. Paired two-tailed Student's t-test, ***$P<0.001$. (D) Lysates from MelJuso cells transfected with control siRNA, siRNAs targeting different regions of TBC1D5, or depleted of TBC1D5 and then transfected with mCherry-TBC1D5 analyzed by western blotting using antibodies against TBC1D5 and tubulin as a loading control. The average percentage of depletion of TBC1D5 was 72% and 65% for siRNA1 and siRNA2, respectively. (E) MelJuso cells stably transfected with GFP-Rab7b were depleted of TBC1D5, and subjected to ultracentrifugation to separate membrane (M) and cytosolic (C) fractions. Lysates were further analyzed by western blotting using an antibody against Rab7b. Antibodies against tubulin and sortilin were used as cytoplasmic and membrane-bound markers, respectively, to control separation between M and C fractions. (F) Quantification of the ratio of membrane-bound and cytosolic Rab7b in MelJuso cells treated with either control siRNA, siRNAs against two different regions of TBC1D5, or cells depleted of TBC1D5 and then transfected with mCherry-TBC1D5. The graph shows the mean±s.e.m. of at least eight independent experiments. Paired two-tailed Student's t-test, *$P<0.05$, **$P<0.01$.

Recent reports, as well as the results from our GTPase activity assay (Fig. 4C), have demonstrated that TBC1D5 also displays GAP activity towards Rab7a (Jia et al., 2016; Jimenez-Orgaz et al., 2018). In order to further compare the effect of TBC1D5 on the binding kinetics of Rab7a and Rab7b to membranes, we performed FRAP experiments by bleaching endosomes positive for either Rab7a or Rab7b, with or without the presence of TBC1D5 (Fig. S4). To bleach single endosomes, we took advantage of the system of Invariant chain (CD74)-enlarged endosomes (Bergeland et al., 2008; Haugen et al., 2017; Nordeng et al., 2002; Skjeldal et al., 2012). The FRAP experiment showed that Rab7b and Rab7a when expressed alone had $t_{1/2}$ recovery of 24.17±0.60 s and 24.74 ±0.59 s, respectively. Intriguingly, when co-expressed with TBC1D5, both Rab7b and Rab7a had a significantly slower $t_{1/2}$ recovery, of 32.06±0.89 s for Rab7b and 31.06±0.43 s for Rab7a (Fig. S4). The mobile fractions (plateau level) showed a similar tendency as the $t_{1/2}$ recovery data. The presence of TBC1D5 diminished the mobile fractions for Rab7a from 72% to 69% and from 75% to 70% for Rab7b. Our results are thus consistent with the reported role of TBC1D5 as a GAP for Rab7a (Jia et al., 2016), and show that TBC1D5 also functions as a GAP for Rab7b on endosomes.

To confirm that TBC1D5 affects the membrane-to-cytosol cycling of Rab7b, we performed a subcellular fractionation assay, where we silenced MelJuso cells stably transfected with GFP-Rab7b with either control siRNA or siRNAs against TBC1D5 (Fig. 5D), and separated the membrane and cytoplasmic fractions by ultracentrifugation. In line with a role for TBC1D5 in promoting Rab7b GTPase activity, the depletion of TBC1D5 caused a significant increase in the amount of membrane-bound Rab7b (Fig. 5E,F). Specifically, the two siRNAs against TBC1D5 caused a 1.5-fold and a 1.7-fold increase in membrane-bound Rab7b, respectively, in comparison to the cells treated with control siRNA (Fig. 5F). The expression of mCherry-TBC1D5 in cells depleted for TBC1D5 reversed this effect and caused a lower membrane-to-cytosol ratio of Rab7b, as in control cells (Fig. 5D-F). These data support a role for TBC1D5 in the inactivation of Rab7b that is required to complete the Rab nucleotide cycle.

TBC1D5 depletion mimics the effects of Rab7b constitutively active mutant

The ability of Rab7b to hydrolyse GTP is important for the proper formation of carriers from the Golgi. Indeed, expression of the constitutively active mutant Rab7b-Q67L causes a marked decrease in the amount of CI-MPR- and sortilin-positive vesicles (Progida et al., 2012). If TBC1D5 is a GAP for Rab7b, its depletion should inhibit Rab7b inactivation, and therefore give a similar effect to the expression of Rab7b-Q67L. To test this, we immunostained cells depleted of TBC1D5 or transfected with GFP-Rab7b-Q76L with antibodies against either CI-MPR or sortilin, counted the number of vesicles positive for these markers relative to numbers in cells treated with control siRNA (Fig. 6). The number of CI-MPR- or sortilin-positive vesicles decreased by ∼30% in cells expressing GFP-Rab7b-Q67L, consistent with previous results (Progida et al., 2012). Interestingly, depletion of TBC1D5 also significantly reduced the number of CI-MPR- or sortilin-positive vesicles. A significant decrease between 20% and 40% compared with control cells was measured for both the two siRNA oligos targeting TBC1D5 (Fig. 6C,D), indicating that TBC1D5 depletion reproduces the effects of defective GTP hydrolysis caused by Rab7b constitutively active mutant. The expression of GFP-TBC1D5 in cells depleted of TBC1D5 restored the number of CI-MPR- or sortilin-positive

vesicles to control levels, again validating the specificity of the silencing (Fig. 6C,D), and TBC1D5 as the actual GAP for Rab7b.

DISCUSSION

In this study, we report the results of an siRNA screen to identify a specific GAP for the small GTPase Rab7b. Rab7b is localized to late endosomes, lysosomes and Golgi, and regulates the retrograde trafficking of different sorting receptors (Progida et al., 2012). We previously showed that the formation of carriers containing sorting receptors from the TGN is impaired when Rab7b is unable to hydrolyse GTP (Progida et al., 2012). As the inactivation of Rab proteins is guided by specific GAPs, which induce the intrinsic GTPase activity of the Rab proteins and thereby their inactivation, here we aimed to identify a specific GAP for Rab7b via a screen of an siRNA library targeting proteins containing a TBC/ Rab-GAP domain.

We hypothesized that after depletion of the specific GAP for Rab7b, this small GTPase is not properly inactivated and therefore localizes mostly in the Golgi, similarly to the GTP-bound constitutively active mutant (Progida et al., 2012). Based on this assumption, after the deconvolution screen we excluded two of the selected candidates, namely TBC1D14 and TBC1D25, as their depletion resulted in a more vesicular distribution of Rab7b. This mislocalization of Rab7b might rather be due to indirect effects of altered pathways regulated by those TBCs rather than a specific GAP activity towards Rab7b. For example, the depletion of TBC1D14 has been shown to cause defects in the retrograde transport of the Shiga toxin (Fuchs et al., 2007). Thus, we can speculate that the dispersion of Rab7b on vesicles after depletion of TBC1D14 is a consequence of the block in the retrograde trafficking route.

After deconvolution and phenotypic evaluation, we identified two Rab7b GAP candidates, TBC1D10A and TBC1D5, which upon silencing, yielded phenotypes similar to that of the constitutively active mutant Rab7b-Q67L, with a more Golgi-associated/ perinuclear distribution of Rab7b (Fig. 2) (Progida et al., 2012).

TBC1D10A, also known as EPI64, has been reported to have GAP activity against other small GTPases, such as Rab27A and Rab35 (Chaineau et al., 2013; Hsu et al., 2010; Itoh and Fukuda, 2006; Nagai et al., 2013). Even though the same GAP protein can act on several Rabs, we found that Rab7b GTPase activity was unaffected by the presence of TBC1D10A (Fig. S3), indicating that this protein is not a specific GAP for Rab7b. In line with this, the $t_{1/2}$ recovery of mCherry-Rab7b after bleaching the Golgi was unaffected in the presence of TBC1D10A (Fig. 5B,C), implying that the mislocalization of Rab7b upon TBC1D10A silencing is most likely an indirect effect of the perturbation in trafficking pathways regulated by this TBC domain-containing protein.

The other GAP selected in the screening was TBC1D5, which is known to interact with the retromer and, like Rab7b, regulates endosome-to-Golgi traffic (Popovic et al., 2012; Progida et al., 2010; Seaman et al., 2009). In line with this, we found that TBC1D5 and Rab7b interact and localize to the same vesicles (Fig. 3).

We applied FRAP technology to measure the effects of TBC1D5 on the Rab7b GTPase cycle in living cells (Langemeyer et al., 2014; Pedro et al., 2017; Reits and Neefjes, 2001). Overexpression of TBC1D5 dramatically diminished the Rab7b binding to the Golgi, indicative of a conversion of Rab7b to its GDP form. On the other hand, we found that the fraction of membrane-bound Rab7b was increased upon depletion of TBC1D5, in comparison to control cells (Fig. 5), further corroborating that TBC1D5 is a Rab7b GAP.

TBC domain-containing GAPs may have multiple target GTPases. TBC1D5 both interacts with and functions as a GAP
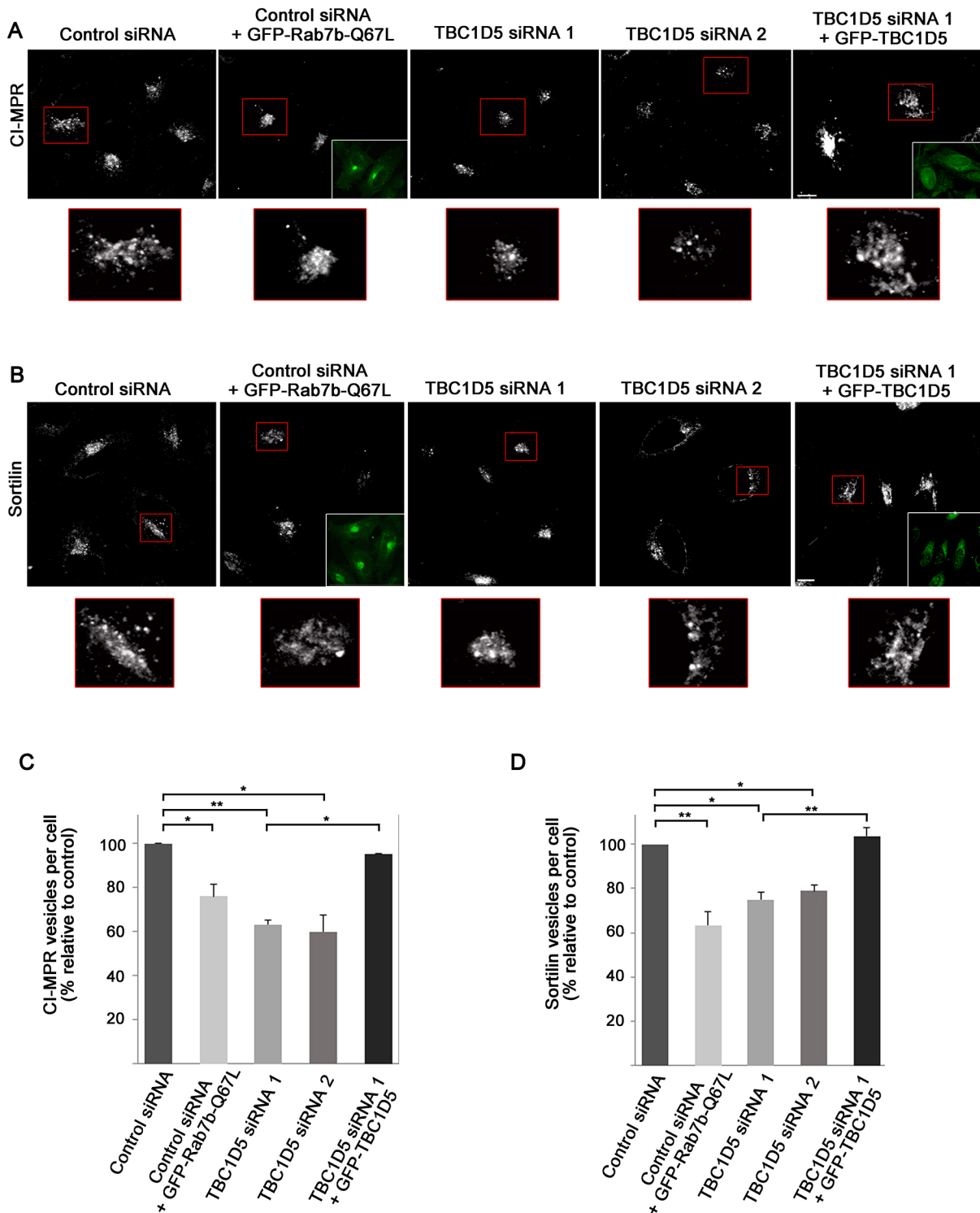
Fig. 6. Depletion of TBC1D5 decreases the number of CI-MPR- and sortilin-positive vesicles. (A,B) HeLa cells transfected with either control siRNA alone or together with GFP-Rab7b-Q67L, or with two different siRNA oligos against TBC1D5, or silenced for TBC1D5 and then transfected with GFP-TBC1D5. The cells were fixed and immunostained with antibodies against CI-MPR (A) or sortilin (B), and analyzed by fluorescent microscopy. Boxed areas are enlarged below. Scale bars: 10 μm. (C,D) The number of CI-MPR-positive (C) or sortilin-positive (D) vesicles for each condition measured using ImageJ shown as a percentage of the total number of vesicles in cells treated with control siRNA. Histogram represents the mean of at least three different experiments±s.e.m. (total $n > 150$ cells), where the average percentage of depletion of TBC1D5 was 76% and 75% for each of the two siRNAs, respectively. Paired two-tailed Student t-test, *$P < 0.05$, **$P < 0.01$.

for Rab7a (Jia et al., 2016). However, TBC1D2 and TBC1D15 have also been described as GAPs for Rab7a (Frasa et al., 2010; Zhang et al., 2005). Indeed, GAP proteins are quite promiscuous and one TBC protein can inactivate several different Rab GTPases (Muller

and Goody, 2017). As such, the fact that TBC1D5 can function as a GAP for Rab7a does not exclude TBC1D5 as a GAP also for Rab7b. Indeed, GTPase activity assays showed that TBC1D5 increases the GTP hydrolysis rate of both Rab7a and Rab7b (Fig. 4C,D).

Similarly, our FRAP results showed that the $t_{1/2}$ recovery of both Rab7a and Rab7b to late endosomes is slower upon co-expression with TBC1D5 (Fig. S4). This suggests that RabGAP proteins also undergo strong regulation to select the inactivation of defined cell biological pathways controlled by the Rab in question. It is likely that the Rab7a and Rab7b cycles link where Rab7a controls normal late endosomal transport and Rab7b transport between the same late endosomes and the Golgi. The observation that TBC1D5 is also found in association with the retromer that indeed provides transport from late endosomes to the Golgi may further substantiate such a link (Jia et al., 2016; Seaman et al., 2009). In fact, the presence of retromer in addition to TBC1D5 further augmented the rate of GTP hydrolysis for Rab7a and Rab7b (Fig. 4C,D).

Both Rab7a and Rab7b GTPases have also been placed at the crossroads of the endosomal system and autophagy. For example, the Rab7-RILP-HOPS complex controls the last step in autophagy – the fusion with late endosomes (Wijdeven et al., 2016). Interestingly, four of the seven hits in our phenotypic screen are also involved in autophagy. TBC1D5 and TBC1D14 both function during autophagosome formation (Lamb et al., 2016; Longatti et al., 2012; Popovic et al., 2012), while TBC1D25 supports the phagosome-lysosome fusion (Itoh et al., 2011) and TBC1D10A inhibits autophagosome biogenesis and maturation (Minowa-Nozawa et al., 2017). We recently identified Rab7b as a negative regulator of autophagy by modulating the activity of the cysteine protease Atg4B (Kjos et al., 2017). Rab7b, via the interaction with Atg4B, could be involved in limiting the expansion of the forming autophagosome. As TBC1D10A, TBC1D5 and TBC1D14 are all important regulators of autophagosome formation, it would be interesting to elucidate in the future if the role of Rab7b in modulating the expansion of autophagosomes is connected to the function of these TBC proteins in autophagy.

Additionally, in recent years, several pathogens have been found to target endosomal retrograde transport pathways to promote their cellular growth and infection (Personnic et al., 2016). The best-characterized example is from *Legionella pneumophila*, the causative agent of Legionnaires' disease. The *L. pneumophila* effector protein RidL directly interacts with retromer, and competes with TBC1D5 *in vitro* and *in vivo* (Bärlocher et al., 2017; Finsel et al., 2013; Romano-Moreno et al., 2017; Yao et al., 2018). Therefore, our findings pave the way for further studies addressing whether RidL and *L. pneumophila* modulate Rab7b-controlled cellular activities.

In sum, we identified TBC1D5 as a regulator of Rab7b cycling. This RabGAP is shared with Rab7a and associates with the retromer. The timing and recruitment of this GAP to endosomes is linked to retromer formation, and by regulating in space and time how Rab7b and its kin, Rab7a, control the endosomal system, TBC1D5 could direct the next phase in transport from late endosomes.

MATERIALS AND METHODS
Cell culture
Wild-type MelJuso cells and MelJuso cells stably transfected with GFP-Rab7b (a gift from Lennert Janssen, The Netherlands Cancer Institute) were grown in Iscove's Modified Dulbecco's Medium (IMDM, Gibco) supplemented with 10% fetal calf serum (FCS, Sigma), 2 mM L-glutamine, 100 U penicillin, 100 µg/ml streptomycin (all from PAA laboratories) and for the stably transfected cells, also 0.8 mg/ml geneticin sulfate (G418, Santa Cruz). Wild-type HeLa cells and MDCK cells stably transfected with Invariant Chain (CD74)-pMep4 (Nordeng et al., 2002; Stang and Bakke, 1997) were grown in Dulbecco's modified Eagle's medium (DMEM, Lonza, Biowhittaker) supplemented with 10% fetal calf serum (FCS, Sigma), 2 mM L-glutamine, 100 U penicillin and 100 µg/ml streptomycin

(all from PAA laboratories) and for the stably transfected cells, also 0.15 mg/ml hygromycin B (Saveen & Werner AB). Invariant chain expression was induced by the addition of 25 µM cadmium chloride in MDCK cells, as previously described (Skjeldal et al., 2012). All cell lines were tested for mycoplasma contamination. MelJuso and HeLa cell lines were authenticated by STR profiling (ATCC).

Constructs and antibodies
The constructs pEGFP-C1-Rab7b, pEGFP-Rab7b-Q67L, pCDNA3.1-mCherry-Rab7a, pCDNA3.1-mCherry-Rab7b, pcDNA2xHA-Rab7b, pcDNA2xHA-Rab7b-Q67L and pcDNA2xHA-Rab7b-T22N have been described previously (Progida et al., 2010, 2012). pEGFP-C2-TBC1D5 and pEGFP-C2-TBC1D10A were a gift from Francis Barr, Department of Biochemistry, University of Oxford, England (Fuchs et al., 2007), and pET60-DEST-TBC1D5 and pHAGE-mCherry-TBC1D5 were a gift from Ivan Dikic, Department of Biochemistry, Goethe University Medical School, Germany (Popovic et al., 2012). Both pEGFP-C2-TBC1D5, pHAGE-mCherry-TBC1D5 and pET60-DEST-TBC1D5 had a point mutation (A in position 2150 instead of T) which was corrected using the QuikChange II XL Site-Directed Mutagenesis Kit (Agilent Technologies) using the following primers: TBC1D5-forward-5′-GAATTCCGATGACTTCATCCTGATTTC-CAAAGATGATGATG-3′ and TBC1D5-reverse 5′-CATCATCATCTTTG-GAAATCAGGATGAAGTCATCGGAATTC-3′. pEGFP-C1 was purchased from BD Biosciences Clontech. pGEX-2T-TBC1D10A was constructed by amplifying TBC1D10A by PCR using the following primers containing, respectively, a *Bam*HI and an *Eco*RI restriction site: TBC1D10A-forward-5′-AGAGAGGATCCATGGCGAAGAGCAACGGAGAG-3′ and TBC1D10-A-reverse 5′-AGAGAGAATTCTTACAAGTAGGTGTCCTCACT-3′. The fragment was then inserted into pGEX-2T that had been digested with *Bam*HI and *Eco*RI. pETM11-Rab7b-WT, pETM11-Rab7b-Q67L and pETM11-Rab7b-T22N were purchased from GenScript.

Antibodies against Rab7b (H00338382-M01, AbNova, 1:300), tubulin (T-9026, Sigma, 1:10,000), GFP (ab6556, Abcam, 1:1000), HA (ab9110, Abcam, 1:500), sortilin (ab24586, Abcam, 1:500), TBC1D5 (17078-1-AP, ProteinTech, 1:500) and TBC1D10A (ab138819, Abcam, 1:100), as well as horseradish peroxidase (HRP)-conjugated secondary antibodies (GE Healthcare and AbD Serotec, 1:5000) were used for western blotting. Antibodies against giantin (ab24586, Abcam, 1:1000), CD63 (NKI-C3, Ventana Medical Systems, 1:50), TBC1D5 (sc99661, Santa Cruz, 1:100), CI-MPR (ab2733, 1:100) and sortilin (ab24586, Abcam, 1:100) were used together with the appropriate Alexa Fluor-conjugated secondary antibodies (Invitrogen, 1:200) for immunofluorescence experiments. Hoechst 33258 (H3569, Life Technologies) was used at 0.2 µg/ml.

RNA interference and transfection
For the siRNA screen, 36 siRNA oligos from the human genome SMARTpool library (Dharmacon, Table S3) were used. MelJuso cells were transfected using the DharmaFect transfection reagent #1 and 50 nm siRNA (Dharmacon) according to the manufacturer's protocol. Briefly, the cells were plated one day prior to transfection in IMDM medium without antibiotics. On the day of transfection, siRNA oligos were added to a 96-well plate followed by addition of Dharmafect Reagent #1 and IMDM without antibiotics or FCS, and lastly 4700 cells per well, to a total volume of 100 µl. 30 µl were transferred to 18-well µ-slides (ibidi® cat. no. 81826), and incubated at 37°C with 5% CO_2 for 72 h.

A scrambled sequence (siRNA control, Dharmacon) was used as a negative control. In addition, positive control siRNAs against PLK1 (important for cell division; Bruinsma et al., 2012) or RNF26 (Ring finger protein 26, known to retain vesicles in the cell periphery; Jongsma et al., 2016), was used to test the silencing efficiency and toxicity (Dharmacon; see Table S3). For deconvolution of the pooled oligos, the respective four individual siRNA oligos (Dharmacon; see Table S3) were tested separately, using the same protocol as previously described.

Transfection of HeLa cells with siRNA was performed as described previously (Progida et al., 2007). Briefly, HeLa cells were plated one day before transfection in 6 cm dishes. Cells were transfected with siRNA using Oligofectamine (Invitrogen) for 72 h, then replated and left for another 48 h before performing experiments.

For overexpression or rescue experiments, MelJuso cells and MDCK cells were transfected with Lipofectamine 2000 transfection reagent (Life Technologies) and HeLa cells using FuGENE 6 (Promega) according to the protocols provided by the manufacturers, and experiments were performed 24 h post transfection.

Immunofluorescence and live cell microscopy

MelJuso cells grown in ibidi® 18-well µ-slides were fixed with 3% paraformaldehyde (PFA) for 15 min. Cells were permeabilized with 0.1% Triton X-100 for 10 min, before blocking for 1 h with 0.5% BSA in 1× PBS. The cells were then incubated with primary antibodies against giantin or CD63 for 1 h followed by Alexa Fluor 555- or Alexa Fluor 647-conjugated secondary antibody for 45 min. The samples were visualized using a Leica AOBS microscope equipped with HCX PL APO 60× objective lenses. The acquisition software used was LEICA LCS.

For vesicle counts, HeLa cells grown on glass coverslips were permeabilized before fixation with 0.25% saponin in 80 mM PIPES and 5 mM EGTA (Sigma) for 2 min. After fixation in 3% PFA, the samples were stained with primary antibodies for 20 min at room temperature, followed by incubation with secondary antibodies for 20 min at room temperature. Mounted coverslips were examined using an Olympus FV1000 confocal laser scanning microscope with a PlanApo 60× oil objective and open pinhole, to allow for the collection of the signal from the entire volume of the cells.

For live cell imaging, cells were grown in 35-mm-diameter imaging dishes with glass bottoms (MatTek), and transfected 24 h prior to the experiment. Cells were imaged in DMEM without Phenol Red, using a 63× PlanApo objective on an Olympus IX-71 microscope equipped with a CSU22 spinning disk confocal unit and an EMCCD camera. During imaging, cells were kept at 37°C with 5% CO_2 in an incubation chamber (Solent Scientific).

Co-immunoprecipitation

GFP-TRAP®_MA for immunoprecipitation of GFP fusion proteins (Chromotek) was used according to the manufacturer's protocol. Briefly, cells were transfected as indicated, and 24 h post-transfection the cells were lysed, washed and incubated for 1 h in end-over-end rotation with magnetic agarose beads. Control beads (nanobodies not coupled to anti-GFP) and a sample transfected with a control vector (pEGFP-C1) were used as negative controls. Immunoprecipitated samples were loaded on SDS-PAGE gels and analysed by western blotting.

Protein expression and purification

Full-length bacterially expressed and purified TBC1D10A was purchased from BioBasic Canada Inc. Constructs for the expression of Rab7b WT and mutants in bacteria were transformed into *E. coli* strain BL21-CodonPlus-DE3-Gold. Bacteria were grown at 37°C in LB medium to OD_{600}=0.6, using a LEX™-48 bioreactor bubbling system (Harbinger Biotechnology and Engineering). The cells were kept on ice for a minimum of 30 min before induction with isopropyl-β-D-thiogalactopyranoside (IPTG) to a final concentration of 0.5 mM. The cells were grown overnight at 22°C, and harvested by centrifugation, before Co^{2+}-column affinity purification, followed by His-tag cleavage and a second Co^{2+}-column affinity purification.

For the GTPase activity assay with TBC1D5 and TBC1D5/retromer, human Rab7a and Rab7b cDNAs were cloned into pGEX-4T1 vector (GE Healthcare). Plasmids were transformed in *E. coli* BL21(DE3)-T1R (Sigma), and proteins were expressed overnight at 25°C. Cells were harvested and sonicated in lysis buffer (20 mM Tris-HCl, pH 8.0, 200 mM NaCl, 2 mM $MgCl_2$, 1 mM PMSF). Proteins were purified on a GST column, and eluted in a buffer containing 100 mM Tris-HCl pH 8.5, 200 mM NaCl, 20 mM glutathione. TBC1D5 (amino acids 1-419) and the TBC1D5-VPS35-VPS29 complex were purified as previously described (Jia et al., 2016). Briefly, VPS35 and VPS29 were individually expressed in *E. coli* BL21(DE3)-T1R, and cell pellets were then mixed and co-lysed. The VPS35-VPS29 complex was purified by the GST-fusion of VPS35, and the GST-fusion was then cleaved by TEV protease. The cleaved VPS35-VPS29 was mixed with TBC1D5 with a molar ratio of 1:2, and excess TBC1D5 was

removed by Source Q ion exchange chromatography (GE Healthcare), yielding a complex of 1:1:1.

In vitro GTPase activity assay

For the GTPase activity assay regarding the Rab7b mutants as well as TBC1D10A, we used the Baginski assay, which measures the amount of Pi released during the reaction by the activity of the GTPase (Baginski et al., 1967). We used a modified Baginski method in which sodium arsenite is replaced with bismuth citrate, and performed the protocol as described previously (Cariani et al., 2004). Briefly, a 60 µl reaction was prepared in a 96-well plate, with 30 µl of 2× assay buffer (40 mM Tris-HCl, pH 8.0, 300 mM NaCl and 10 mM $MgCl_2$), 12 µM purified Rab7b, and 1 µM of the purified TBCs in the indicated samples. The mix was preincubated for 10 min at 37°C, before starting the reaction by adding 1 mM GTP and incubating for 1 h at 37°C. The reaction was terminated and phosphate content was detected by adding 75 µl of Solution I (prepared on the same day by dissolving 0.3 g of ascorbic acid in 3.5 ml water, followed by adding 5 ml of 1 M HCl, 0.5 ml of 10% ammonium molybdate and 1.5 ml of 20% SDS). The terminated reaction mix was incubated for 10 min on ice before adding 125 µl of solution II (3.5% sodium citrate and 3.5% bismuth citrate in 1 M HCl) and incubated at room temperature (RT) for an additional 10 min. Absorbance was measured at 690 nm with Infinite F200 PRO microplate reader and compared with the Pi standard curve.

For the GTPase activity assay of Rab7a and Rab7b with and without TBC1D5 and retromer components, Rab7a and Rab7b proteins were charged with GTP as previously described (Jia et al., 2016). Free nucleotides were then removed by a desalting column, and freshly charged proteins were immediately used for the assays carried out at RT. The final solution contained 20 mM HEPES, pH 7.5, 150 mM NaCl, 20 µM Rab7a or Rab7b, and 400 nM TBC1D5 or TBC1D5-VPS35-VPS29. At each time point, reaction solution (50 µl) was mixed with Malachite Green reagent (100 µl, BioAssay Systems, USA), which also terminated the reaction. After incubation at RT for 15 min, phosphate release was determined by measuring absorbance at 620 nm.

Subcellular fractionation assay

MelJuso cells were washed with 1× PBS, collected and centrifuged at 1300 *g* for 5 min at 4°C, before addition of 250 µl homogenizer buffer (8% sucrose, 3 mM imidazole and 1:100 protease inhibitor) to each sample. A 27 G syringe was used to lyse the cells, before centrifugation at 3800 *g* for 5 min at 4°C to pellet the nuclei. The supernatant was further centrifuged at 100,000 *g* for 1 h at 4°C, using a TLA 100.1 rotor (Beckman Coulter). After ultracentrifugation, supernatant (i.e. cytosol) and pellet (i.e. membranes) were carefully separated and subjected to western blot analysis.

SDS-PAGE and immunoblotting

After protein purification, proteins were separated by SDS-PAGE and stained with Coomassie Blue. For western blot experiments, proteins were separated using SDS-PAGE, transferred to an Immobilion™ Polyvinylidene fluoride (PVDF) membrane (Millipore), and incubated overnight with primary antibodies at 4°C. After washing, the membrane was incubated with horseradish peroxidase (HRP)-conjugated secondary antibodies for 1 h. Protein bands were detected by using Amersham™ ECL Plus Western Blotting Detection System. Band intensity was quantified using ImageQuant TL software (GE Healthcare).

Fluorescence recovery after photobleaching (FRAP)

FRAP was performed at 37°C with 5% CO_2 using an inverted Olympus iX81 FluoView 1000 confocal microscope (Olympus, Hamburg, DE), equipped with a PlanApo 60×/1.10 oil immersion objective. This microscope has a 4-channel PMT detector unit and a dual SIM scanner specifically designed for high speed FRAP analysis (Bergeland, 2006). GFP was imaged with the multilane Argon laser (457 nm, 488 nm and 515 nm) and mCherry with the 559 nm laser. The 559 nm laser was used with maximum laser power to bleach mCherry-Rab7b localized in the Golgi for 3500 ms, or to bleach mCherry-Rab7a or mCherry-Rab7b on enlarged endosomes for 2000 ms. Recovery was measured by acquiring images every 1.6 s for 12 frames, and further by taking images every 30 s for 60 frames for Golgi FRAP experiments, and by

acquiring images every 0.7 s for 12 frames and further taking images every minute for 15 frames for endosome FRAP experiments.

The obtained data were normalized and corrected for bleaching (Pelkmans et al., 2001) and fitted by nonlinear regression to a function that assumes a single diffusion coefficient (Yguerabide et al., 1982):

$$F_t = \frac{F_0 + F_\infty (t/t_{1/2})}{1 + (t/t_{1/2})} \qquad (1)$$

The values for F_0, F_∞ and $t_{1/2}$ were calculated as described in Lippincott-Schwartz et al. (2001) and using GraphPad Prism 6 (http://www.graphpad.com/scientific-software/prism/).

Image analysis, processing and statistical analysis

Immunofluorescence imaging experiments were quantified observers blinded to the experiment when possible to minimize bias. Images were processed with ImageJ and Adobe Photoshop. The size or number of vesicles was calculated after background subtraction and thresholding using the Analyze Particle feature of ImageJ. The analysis of TBC1D5 and Rab7b co-localization was performed in ImageJ by drawing a line across the membrane of a vesicle. The profiles of fluorescence intensities along the drawn line were obtained for each channel for the different time points. Statistical differences, unless otherwise stated, were assessed by two-tailed paired Student's t-test (GraphPad software and Excel software). In the figures, statistical significance is indicated as follows: $*P<0.05$, $**P<0.01$, $***P<0.001$.

References
Baginski, E. S., Foa, P. P. and Zak, B. (1967). Microdetermination of inorganic phosphate, phospholipids, and total phosphate in biologic materials. *Clin. Chem.* **13**, 326-332.

Bärlocher, K., Hutter, C. A. J., Swart, A. L., Steiner, B., Welin, A., Hohl, M., Letourneur, F., Seeger, M. A. and Hilbi, H. (2017). Structural insights into Legionella RidL-Vps29 retromer subunit interaction reveal displacement of the regulator TBC1D5. *Nat. Commun.* **8**, 1543.

Barr, F. and Lambright, D. G. (2010). Rab GEFs and GAPs. *Curr. Opin. Cell Biol.* **22**, 461-470.

Bergeland, T. (2006). Precise calculation of photoactivation kinetics. *Nat. Methods* **3**, 2042-2043. https://www.nature.com/app_notes/nmeth/2006/062811/full/nmeth982.html

Bergeland, T., Haugen, L., Landsverk, O. J. B., Stenmark, H. and Bakke, O. (2008). Cell-cycle-dependent binding kinetics for the early endosomal tethering factor EEA1. *EMBO Rep.* **9**, 171-178.

Borg, M., Bakke, O. and Progida, C. (2014). A novel interaction between Rab7b and actomyosin reveals a dual role in intracellular transport and cell migration. *J. Cell Sci.* **127**, 4927-4939.

Bruinsma, W., Raaijmakers, J. A. and Medema, R. H. (2012). Switching Polo-like kinase-1 on and off in time and space. *Trends Biochem. Sci.* **37**, 534-542.

Cariani, L., Thomas, L., Brito, J. and del Castillo, J. R. (2004). Bismuth citrate in the quantification of inorganic phosphate and its utility in the determination of membrane-bound phosphatases. *Anal. Biochem.* **324**, 79-83.

Chaineau, M., Ioannou, M. S. and McPherson, P. S. (2013). Rab35: GEFs, GAPs and effectors. *Traffic* **14**, 1109-1117.

Finsel, I., Ragaz, C., Hoffmann, C., Harrison, C. F., Weber, S., van Rahden, V. A., Johannes, L. and Hilbi, H. (2013). The Legionella effector RidL inhibits retrograde trafficking to promote intracellular replication. *Cell Host Microbe* **14**, 38-50.

Frasa, M. A. M., Maximiano, F. C., Smolarczyk, K., Francis, R. E., Betson, M. E., Lozano, E., Goldenring, J., Seabra, M. C., Rak, A., Ahmadian, M. R. et al. (2010). Armus is a Rac1 effector that inactivates Rab7 and regulates E-cadherin degradation. *Curr. Biol.* **20**, 198-208.

Fuchs, E., Haas, A. K., Spooner, R. A., Yoshimura, S., Lord, J. M. and Barr, F. A. (2007). Specific Rab GTPase-activating proteins define the Shiga toxin and epidermal growth factor uptake pathways. *J. Cell Biol.* **177**, 1133-1143.

Gavriljuk, K., Gazdag, E.-M., Itzen, A., Kotting, C., Goody, R. S. and Gerwert, K. (2012). Catalytic mechanism of a mammalian Rab.RabGAP complex in atomic detail. *Proc. Natl. Acad. Sci. USA* **109**, 21348-21353.

Grosshans, B. L., Ortiz, D. and Novick, P. (2006). Rabs and their effectors: achieving specificity in membrane traffic. *Proc. Natl. Acad. Sci. USA* **103**, 11821-11828.

Hanono, A., Garbett, D., Reczek, D., Chambers, D. N. and Bretscher, A. (2006). EPI64 regulates microvillar subdomains and structure. *J. Cell Biol.* **175**, 803-813.

Haugen, L. H., Skjeldal, F. M., Bergeland, T. and Bakke, O. (2017). Endosomal binding kinetics of Eps15 and Hrs specifically regulate the degradation of RTKs. *Sci. Rep.* **7**, 17962.

Hsu, C., Morohashi, Y., Yoshimura, S., Manrique-Hoyos, N., Jung, S. Y., Lauterbach, M. A., Bakhti, M., Grønborg, M., Möbius, W., Rhee, J. S. et al. (2010). Regulation of exosome secretion by Rab35 and its GTPase-activating proteins TBC1D10A-C. *J. Cell Biol.* **189**, 223-232.

Itoh, T. and Fukuda, M. (2006). Identification of EPI64 as a GTPase-activating protein specific for Rab27A. *J. Biol. Chem.* **281**, 31823-31831.

Itoh, T., Kanno, E., Uemura, T., Waguri, S. and Fukuda, M. (2011). OATL1, a novel autophagosome-resident Rab33B-GAP, regulates autophagosomal maturation. *J. Cell Biol.* **192**, 839-853.

Jia, D., Zhang, J.-S., Li, F., Wang, J., Deng, Z., White, M. A., Osborne, D. G., Phillips-Krawczak, C., Gomez, T. S., Li, H. et al. (2016). Structural and mechanistic insights into regulation of the retromer coat by TBC1d5. *Nat. Commun.* **7**, 13305.

Jimenez-Orgaz, A., Kvainickas, A., Nägele, H., Denner, J., Eimer, S., Dengjel, J. and Steinberg, F. (2018). Control of RAB7 activity and localization through the retromer-TBC1D5 complex enables RAB7-dependent mitophagy. *EMBO J.* **37**, 235-254.

Jongsma, M. L. M., Berlin, I., Wijdeven, R. H. M., Janssen, L., Janssen, G. M. C., Garstka, M. A., Janssen, H., Mensink, M., van Veelen, P. A., Spaapen, R. M. et al. (2016). An ER-associated pathway defines endosomal architecture for controlled cargo transport. *Cell* **166**, 152-166.

Kjos, I., Borg Distefano, M., Saetre, F., Repnik, U., Holland, P., Jones, A. T., Engedal, N., Simonsen, A., Bakke, O. and Progida, C. (2017). Rab7b modulates autophagic flux by interacting with Atg4B. *EMBO Rep.* **18**, 1727-1739.

Lamb, C. A., Nühlen, S., Judith, D., Frith, D., Snijders, A. P., Behrends, C. and Tooze, S. A. (2016). TBC1D14 regulates autophagy via the TRAPP complex and ATG9 traffic. *EMBO J.* **35**, 281-301.

Langemeyer, L., Nunes Bastos, R., Cai, Y., Itzen, A., Reinisch, K. M. and Barr, F. A. (2014). Diversity and plasticity in Rab GTPase nucleotide release mechanism has consequences for Rab activation and inactivation. *eLife* **3**, e01623.

Lippincott-Schwartz, J., Snapp, E. and Kenworthy, A. (2001). Studying protein dynamics in living cells. *Nat. Rev. Mol. Cell Biol.* **2**, 444-456.

Longatti, A., Lamb, C. A., Razi, M., Yoshimura, S., Barr, F. A. and Tooze, S. A. (2012). TBC1D14 regulates autophagosome formation via Rab11- and ULK1-positive recycling endosomes. *J. Cell Biol.* **197**, 659-675.

Minowa-Nozawa, A., Nozawa, T., Okamoto-Furuta, K., Kohda, H. and Nakagawa, I. (2017). Rab35 GTPase recruits NPD52 to autophagy targets. *EMBO J.* **36**, 2790-2807.

Mishra, A. K. and Lambright, D. G. (2015). High-throughput assay for profiling the substrate specificity of Rab GTPase-activating proteins. *Methods Mol. Biol.* **1298**, 47-60.

Mukhopadhyay, A., Pan, X., Lambright, D. G. and Tissenbaum, H. A. (2007). An endocytic pathway as a target of tubby for regulation of fat storage. *EMBO Rep.* **8**, 931-938.

Muller, M. P. and Goody, R. S. (2017). Molecular control of Rab activity by GEFs, GAPs and GDI. *Small GTPases* **9**, 5-21.

Nagai, H., Yasuda, S., Ohba, Y., Fukuda, M. and Nakamura, T. (2013). All members of the EPI64 subfamily of TBC/RabGAPs also have GAP activities towards Ras. *J. Biochem.* **153**, 283-288.

Nordeng, T. W., Gregers, T. F., Kongsvik, T. L., Méresse, S., Gorvel, J.-P., Jourdan, F., Motta, A. and Bakke, O. (2002). The cytoplasmic tail of invariant chain regulates endosome fusion and morphology. *Mol. Biol. Cell* **13**, 1846-1856.

Pan, X., Eathiraj, S., Munson, M. and Lambright, D. G. (2006). TBC-domain GAPs for Rab GTPases accelerate GTP hydrolysis by a dual-finger mechanism. *Nature* **442**, 303-306.

Paul, P. and Neefjes, J. (2013). Studying MHC class II transport in dendritic cells. *Methods Mol. Biol.* **960**, 489-507.

Pedro, M. P., Vilcaes, A. A., Gomez, G. A. and Daniotti, J. L. (2017). Individual S-acylated cysteines differentially contribute to H-Ras endomembrane trafficking and acylation/deacylation cycles. *Mol. Biol. Cell* **28**, 962-974.

Pelkmans, L., Kartenbeck, J. and Helenius, A. (2001). Caveolar endocytosis of simian virus 40 reveals a new two-step vesicular-transport pathway to the ER. *Nat. Cell Biol.* **3**, 473-483.

Personnic, N., Bärlocher, K., Finsel, I. and Hilbi, H. (2016). Subversion of retrograde trafficking by translocated pathogen effectors. *Trends Microbiol.* **24**, 450-462.

Popovic, D., Akutsu, M., Novak, I., Harper, J. W., Behrends, C. and Dikic, I. (2012). Rab GTPase-activating proteins in autophagy: regulation of endocytic and autophagy pathways by direct binding to human ATG8 modifiers. *Mol. Cell. Biol.* **32**, 1733-1744.

Progida, C., Malerod, L., Stuffers, S., Brech, A., Bucci, C. and Stenmark, H. (2007). RILP is required for the proper morphology and function of late endosomes. *J. Cell Sci.* **120**, 3729-3737.

Progida, C., Cogli, L., Piro, F., De Luca, A., Bakke, O. and Bucci, C. (2010). Rab7b controls trafficking from endosomes to the TGN. *J. Cell Sci.* **123**, 1480-1491.

Progida, C., Nielsen, M. S., Koster, G., Bucci, C. and Bakke, O. (2012). Dynamics of Rab7b-dependent transport of sorting receptors. *Traffic* **13**, 1273-1285.

Pylypenko, O., Hammich, H., Yu, I. M. and Houdusse, A. (2017). Rab GTPases and their interacting protein partners: structural insights into Rab functional diversity. *Small GTPases* **9**, 22-48.

Reits, E. A. J. and Neefjes, J. J. (2001). From fixed to FRAP: measuring protein mobility and activity in living cells. *Nat. Cell Biol.* **3**, E145-E147.

Romano-Moreno, M., Rojas, A. L., Williamson, C. D., Gershlick, D. C., Lucas, M., Isupov, M. N., Bonifacino, J. S., Machner, M. P. and Hierro, A. (2017). Molecular mechanism for the subversion of the retromer coat by the Legionella effector RidL. *Proc. Natl. Acad. Sci. USA* **114**, E11151-E11160.

Seaman, M. N. J., Harbour, M. E., Tattersall, D., Read, E. and Bright, N. (2009). Membrane recruitment of the cargo-selective retromer subcomplex is catalysed by the small GTPase Rab7 and inhibited by the Rab-GAP TBC1D5. *J. Cell Sci.* **122**, 2371-2382.

Skjeldal, F. M., Strunze, S., Bergeland, T., Walseng, E., Gregers, T. F. and Bakke, O. (2012). The fusion of early endosomes induces molecular-motor-driven tubule formation and fission. *J. Cell Sci.* **125**, 1910-1919.

Stang, E. and Bakke, O. (1997). MHC class II-associated invariant chain-induced enlarged endosomal structures: a morphological study. *Exp. Cell Res.* **235**, 79-92.

Stenmark, H. (2009). Rab GTPases as coordinators of vesicle traffic. *Nat. Rev. Mol. Cell Biol.* **10**, 513-525.

Wijdeven, R. H., Janssen, H., Nahidiazar, L., Janssen, L., Jalink, K., Berlin, I. and Neefjes, J. (2016). Cholesterol and ORP1L-mediated ER contact sites control autophagosome transport and fusion with the endocytic pathway. *Nat. Commun.* **7**, 11808.

Wubbolts, R., Fernandez-Borja, M., Oomen, L., Verwoerd, D., Janssen, H., Calafat, J., Tulp, A., Dusseljee, S. and Neefjes, J. (1996). Direct vesicular transport of MHC class II molecules from lysosomal structures to the cell surface. *J. Cell Biol.* **135**, 611-622.

Yang, M., Chen, T., Han, C., Li, N., Wan, T. and Cao, X. (2004). Rab7b, a novel lysosome-associated small GTPase, is involved in monocytic differentiation of human acute promyelocytic leukemia cells. *Biochem. Biophys. Res. Commun.* **318**, 792-799.

Yao, J., Yang, F., Sun, X., Wang, S., Gan, N., Liu, Q., Liu, D., Zhang, X., Niu, D., Wei, Y. et al. (2018). Mechanism of inhibition of retromer transport by the bacterial effector RidL. *Proc. Natl. Acad. Sci. USA* **115**, E1446-E1454.

Yguerabide, J., Schmidt, J. A. and Yguerabide, E. E. (1982). Lateral mobility in membranes as detected by fluorescence recovery after photobleaching. *Biophys. J.* **40**, 69-75.

Zhang, X.-M., Walsh, B., Mitchell, C. A. and Rowe, T. (2005). TBC domain family, member 15 is a novel mammalian Rab GTPase-activating protein with substrate preference for Rab7. *Biochem. Biophys. Res. Commun.* **335**, 154-161.